The Impact of Ozone Production on Future Cold Point Tropopause Warming and Expansion

Stephen Bourguet[1]

[1]Harvard University

August 12, 2023

Abstract

A robust thermodynamic response of increased greenhouse gas forcing is an expansion of the troposphere, which may decrease ozone concentrations in the lower stratosphere and warm the tropopause. Yet, observations of lower stratospheric ozone do not agree with model projections, and the net effect of greenhouse gas forcing on the temperature structure of the region between the tropical troposphere and stratosphere is unclear. Here, I isolate the role of local ozone production in setting the height of the cold point tropopause and the ozone concentrations above this level. Increased ozone production near the tropopause following tropospheric expansion will sharpen the vertical ozone gradient of the lower stratosphere and decrease the distance between the top of the troposphere and the cold point tropopause. This would suppress tropospheric expansion and increase the water vapor concentration of the stratosphere, which amplifies global warming and contributes to stratospheric ozone destruction.

The Impact of Ozone Production on Future Cold Point Tropopause Warming and Expansion

Stephen Bourguet

[1]Harvard University, Department of Earth and Planetary Sciences, Harvard University, Cambridge, MA 02138, USA

Key Points:

- Ozone concentrations at the cold point tropopause and above 30 hPa in the tropics are approximately constant throughout the year.
- At the cold point tropopause, this concentration is determined by the origin of air and in-situ ozone production.
- Increases to the cold point tropopause height will increase local ozone production, inducing local warming and limiting further expansion.

Corresponding author: Stephen Bourguet, `Stephen_Bourguet@g.harvard.edu`

Abstract

A robust thermodynamic response of increased greenhouse gas forcing is an expansion of the troposphere, which may decrease ozone concentrations in the lower stratosphere and warm the tropopause. Yet, observations of lower stratospheric ozone do not agree with model projections, and the net effect of greenhouse gas forcing on the temperature structure of the region between the tropical troposphere and stratosphere is unclear. Here, I isolate the role of local ozone production in setting the height of the cold point tropopause and the ozone concentrations above this level. Increased ozone production near the tropopause following tropospheric expansion will sharpen the vertical ozone gradient of the lower stratosphere and decrease the distance between the top of the troposphere and the cold point tropopause. This would suppress tropospheric expansion and increase the water vapor concentration of the stratosphere, which amplifies global warming and contributes to stratospheric ozone destruction.

Plain Language Summary

As greenhouse gas emissions warm the earth's surface, the lowermost layer of the atmosphere will expand upwards and the middle atmosphere will cool and shrink. The effect of these changes on the ozone and temperature profiles of the region that bridges the lower and middle atmosphere has been studied previously, but there is still some debate on how these profiles will evolve. Here, I show how ozone production, which does not depend on the height of atmospheric layers, will increase within this transition region, thereby increasing its ozone concentration. This helps explain discrepancies between model projections of ozone concentrations and observations. Additionally, increased ozone concentrations will increase the temperature of air entering the stratosphere, which allows this air to hold more water vapor and has important implications for atmospheric chemistry and global warming.

1 Introduction

Tropical lower stratospheric ozone concentrations are projected to decrease following surface warming (Eyring et al., 2010), but observed decreases over the past two decades are insignificant when considering changes to tropopause height (Thompson et al., 2021). This is part of broader disagreement between ozone projections in chemistry-climate models and observations which needs to be reconciled in order to understand the recovery of the protective stratospheric ozone layer following the Montreal Protocol's global ban on halogen-containing ozone depleting substances in the late 1990s (Ball et al., 2020).

The ozone profile between the tropical tropopause and the lower stratosphere also influences atmospheric circulation and chemistry and surface climate (Ming et al., 2016). Near the tropical tropopause, ozone is a strong absorber of longwave radiation, and the temperature structure of the tropical tropopause layer (TTL) is sensitive to ozone concentrations therein (Birner & Charlesworth, 2017). This contributes to the strong static stability of the tropopause inversion layer and the lower stratosphere (Grise et al., 2010), as well as the extreme cold temperatures of the TTL which dehydrate air as it fills the stratosphere (Brewer, 1949). Water vapor impacts ozone chemistry and is a strong greenhouse gas near the tropopause (Dvortsov & Solomon, 2001; Solomon et al., 2010), and climate models project an increase in lower stratospheric water vapor with surface warming (Gettelman et al., 2010; Keeble et al., 2021). Yet, these models cannot reproduce observations, and ozone concentrations have been identified as a driver of intermodel disagreement (Gettelman et al., 2009).

The response of lower stratospheric ozone to greenhouse gas forcing is complex. Tropospheric expansion, which is a robust thermodynamic consequence of surface warming, will not simply shift the stratospheric ozone profile upwards by the extent that the tropopause is displaced. Instead, the lower stratospheric ozone profile will be pushed upwards, while ozone concentrations in regions dominated by photochemistry will be unaffected by the transport of ozone-poor air from below (Perliski et al., 1989). In the absence of changes to upwelling or production, tropopause-following coordinates would eliminate any changes to lower stratospheric ozone, while an accelerated Brewer-Dobson circulation would enhance the transport of ozone-poor air into the stratosphere and decrease ozone concentrations in the region above the tropopause (Match & Gerber, 2022). On the other hand, changes to the ozone production rate could increase ozone concentrations in this region where the transport of ozone-poor air is balanced by local ozone production. Although ozone production in the lower stratosphere is weak, it strengthens rapidly with height, so the ozone concentration at the tropopause should be sensitive to its height.

Here, I explore how changes to ozone production following tropospheric expansion above the level of zero radiative heating (LZRH) could impact ozone concentrations in this region and alter the thermodynamic environment of the TTL. I do so by first establishing a budget for the ozone concentration at the cold point tropopause. I then construct ozone profiles that follow from tropospheric expansion with this budget and use a radiative transfer code to calculate corresponding changes to TTL temperatures and water vapor concentrations. Finally, I test the robustness of this mechanism to changes in tropical stratospheric upwelling.

2 Data and Methods

2.1 Ozone Data

Monthly-mean zonal-mean ozone profiles from the Stratospheric Water and OzOne Satellite Homogenized data set (SWOOSH, Davis et al. (2016)) were used to construct an ozone budget for the cold point tropopause. These data are on a pressure grid with two levels near the cold point tropopause (100 hPa and 82.5 hPa), so the ozone concentrations were interpolated to the cold point tropopause height diagnosed from monthly mean temperatures from the European Center for Medium-range Weather Forecasts latest reanalysis product, ERA5 (Hersbach et al., 2020), and the Radio Occultation Meteorology Satellite Application Facility's multi-mission data set (Ho et al., 2012; Steiner et al., 2013; Gleisner et al., 2020). This was done for 2002 to 2016, which are the years that all datasets were available.

Ozone production rates were taken from the Community Earth Systems Model's Whole Atmosphere Chemistry and Composition Model (CESM1 WACCM4). For the base state, an average over 2004 to 2009 was used (data are described in Abalos et al. (2013)). For two surface warming scenarios, uniform temperature increases of 3 and 5 K were imposed with CO_2 concentrations of 560 and 1000 ppm, respectively. Zonal mean ozone production for each of these scenarios is shown in Figure S1.

2.2 The Lagrangian Framework

Ozone concentrations within the TTL balance the advection of ozone-poor air from the troposphere with in-mixing of ozone-rich air from the extratropical lower stratosphere and in-situ photochemical production (Abalos et al., 2013). Therefore, the Lagrangian trajectory model LAGRANTO (Sprenger & Wernli, 2015) was used to trace the origin of air masses that ascend to the cold point tropopause and the path they take to calculate the cold point tropopause's ozone budget. Following the procedure of Bourguet and Linz (2022), reverse trajectories were initialized from 20°S to 20°N at all longitudes with 0.5° spacing on the last day of February and the last day of August in 2007, 2008, and 2009 near the cold point tropopause (90 hPa in boreal winter and 100 hPa in boreal summer). ERA5 hourly winds were used and trajectories were traced backwards for 90 days.

Using trajectory distributions, I construct the following budget for the cold point tropopause's ozone concentration:

$$O3_{c.p.} = O3_{initial} + \text{Net Production} + \text{Residual Mixing}. \quad (1)$$

The "initial" ozone concentration ($O3_{initial}$) depends on the timescale of interest – here, this is the average ozone concentration at the trajectories' locations at the end of integration (90 days prior to reaching the cold point tropopause). This was calculated using a weighted average of SWOOSH ozone concentrations, with the weighting determined by trajectory distributions. The net production term was calculated using trajectory weightings at the end of each day, with the net ozone production field taken from WACCM's zonal mean net ozone tendency.

"Residual" or sub-grid scale mixing can be diagnosed with this framework by comparing the observed cold point tropopause ozone concentration to the concentration calculated by Eq. 1 without mixing. To do so, ozone concentrations were initialized based on trajectory distributions 90 days prior to reaching the cold point tropopause and then increased each day according to the trajectories' average ozone tendency. Disagreement between the constructed ozone concentration at the end of the timeseries (the end of February or August) and the observed ozone concentrations were assumed to be caused by mixing that the Lagrangian framework cannot capture. In 2007, 2008, and 2009 respectively, the residual mixing terms were –3%, –8%, and –4% of the cold point tropopause's ozone concentration in February and 2%, —1%, and 14% in August. Thus, Eq. 1 can be reduced to:

$$O3_{c.p.} \approx O3_{initial} + \text{Net Production}. \quad (2)$$

2.3 Idealized Tropospheric Expansion

The following experiments are idealized representations of 3 and 5 K of surface warming, which would drive approximately 18 and 30 hPa of tropospheric expansion, respectively (Match & Fueglistaler, 2021). The results shown in the text are for 5 K of warming; corresponding plots for 3 K are shown in the supplemental.

2.3.1 Changes to Ozone at the Cold Point Tropopause

To calculate how ozone concentrations at the cold point tropopause will change with surface warming, it was assumed that in-mixing from the extratropics follows the tropopause upwards. Anticipated increases in the meridional ozone gradient (Shepherd, 2008) and mixing rates (Abalos et al., 2017) would increase the in-mixing of ozone, thereby making this a conservative treatment of future in-mixing. Tropospheric ozone concentrations were also assumed to remain negligible, which is reasonable given the lifetime of ozone in the troposphere (Wild, 2007). These assumptions simplify the time derivative of Eq. 2 to:

$$\Delta O3_{c.p.} = \Delta \text{Net Production}. \quad (3)$$

Trajectory distributions from 2008 with their pressure offset by the rate of tropospheric expansion were used to calculate ΔNet Production. This assumes that the path of air en route to the cold point tropopause will follow the tropopause upwards, which is consistent with the assumption of constant in-mixing from the extratropics. As discussed in Sections 2.1, the future zonal mean net ozone production rates are calculated using WACCM.

2.3.2 Temperature and Water Vapor

The radiative transfer code RRTMG (Mlawer et al., 1997; Kluft et al., 2019) with fixed dynamic heating was used to calculate how cold point tropopause pressures and temperatures will respond to changes in the ozone profiles following tropospheric expansion. To do so, the modified ozone profile was taken from Section 4.1, and the dynamic heating profile was shifted upwards according to the rate of tropospheric expansion. Temperatures beneath the LZRH were increased by 3 or 5 K, and the CO_2 concentrations were increased to 560 and 1000 ppm for the two experiments, respectively. Stratospheric water vapor concentrations were calculated based on Clausius-Clapeyron relationship at the cold point tropopause at each timestep. Additional details are given in Text S1.

3 Observed Cold Point Tropopause Ozone Concentrations

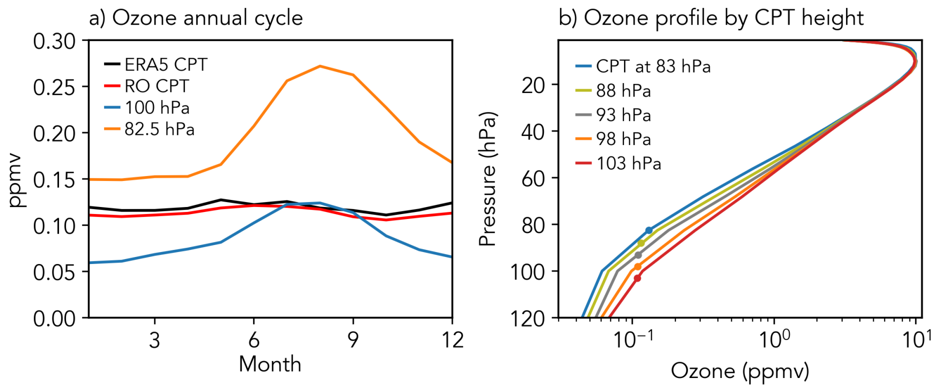

Figure 1. a) The annual cycle of zonal mean (15°S to 15°N) SWOOSH ozone concentrations at 100 hPa (blue line), 82.5 hPa (orange line), and the cold point tropopause interpolated from monthly mean radio occultations (red line) and ERA5 temperature profiles (black line). b) SWOOSH ozone profiles organized by ERA5 cold point tropopause height with the ozone concentration at the cold point tropopause marked with circles.

Figure 1a shows that the ozone concentration at the cold point tropopause is approximately constant throughout the year, while the concentrations at nearby pressure levels vary between the solstices. In the TTL, ozone concentrations at fixed heights will vary as the transport of ozone-poor air varies (Randel et al., 2007), leading to temperature changes that reinforce those already driven by variations in dynamic cooling (Birner & Charlesworth, 2017). The cold point tropopause is able to follow these changes to dynamic and radiative heating, resulting in its position on a fixed ozone surface.

SWOOSH ozone profiles are separated by the ERA5 cold point tropopause height in Figure 1b. These profiles emphasize the variance of lower stratospheric ozone concentrations as the cold point tropopause moves up and down in height. Ozone concentrations beneath 30 hPa covary with the movement of the cold point tropopause, while concentrations above 30 hPa are insensitive to lower stratospheric ozone variability. This reflects the division of stratospheric ozone into regimes of balanced transport and production in the lower to middle stratosphere and balanced production and loss in the middle to upper stratosphere (Perliski et al., 1989). Ozone concentrations at the cold point tropopause (highlighted by circles in Figure 1b) vary by less than 0.01 ppmv as the cold point tropopause height varies by 20 hPa.

These observations reveal a previously overlooked feature of the cold point tropopause in the modern climate: a fixed ozone concentration of about 0.12 ppmv. Given the seasonal and interannual fluctuations in the height of the cold point tropopause, this feature prompts the usage of cold point-relative coordinates to understand the ozone budget of the cold point tropopause and lowermost stratosphere.

4 Tropospheric Expansion

4.1 Ozone Profiles

To create ozone profiles that emulate the effect of 30 hPa of tropospheric expansion without increased ozone production beneath the cold point tropopause, ozone profiles were shifted up by 30 hPa and then tapered back to observations between the cold point tropopause and 30 hPa. This decreases ozone concentrations at fixed heights in the lower to middle stratosphere but does not change concentrations in tropopause-following coordinates. Ozone concentrations above 30 hPa were increased by 10% to simulate the decrease in odd-oxygen loss that would result from stratospheric cooling (Jonsson et al., 2004). (The increase aloft is not a result of tropospheric expansion but does impact TTL thermodynamics and ozone production by blocking shortwave radiation. Subsequent results are not sensitive to the choice of amplification within the range of model projections (Chiodo et al., 2018).)

To include increased ozone production between the LZRH and the cold point tropopause, the ozone concentration at the height 30 hPa above the modern cold point tropopause was calculated using Eq. 3. This would be the ozone concentration at the cold point tropopause if changes to its height were set by dynamics above the LZRH and not thermodynamics. Ozone concentrations were then increased from observations at the LZRH to this increased value at the lifted cold point tropopause.

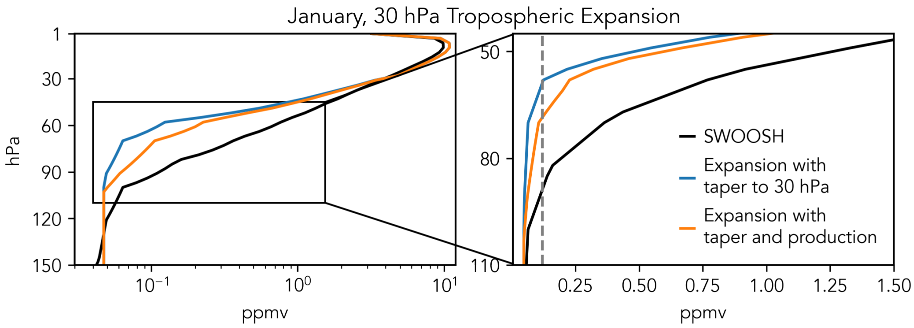

Figure 2. The 2002–2016 mean January ozone profile taken from SWOOSH (black line) and ozone profiles following 30 hPa of tropospheric expansion with and without increased ozone production (orange and blue, respectively). The 45 to 110 hPa layer is reproduced in the right panel to show the large difference near the cold point tropopause. The corresponding July ozone profile and profiles for 15 hPa of tropospheric expansion are shown in Figure S2.

The profiles for January following 30 hPa of tropospheric expansion are shown by the blue (expansion only) and orange (expansion and increased production) lines in Figure 2, with the modern ozone profile shown in black. By construction, these profiles are qualitatively similar to those in Figure 1b. In both cases, ozone varies with tropopause height in the region where transport and production are balanced, but the difference between the ozone profiles in Figure 2 comes from differences in production, rather than transport. In the right panel, which focuses on the TTL, a vertical line at the ozone concentration of the modern cold point tropopause (about 0.12 ppmv) is included to highlight where the cold point tropopause would be if it were to follow the same ozone concentration level as the troposphere expands.

4.2 Cold Point Tropopause Temperature and Water Vapor

Using the ozone profile shown in Figure 2 and the corresponding profile for JJA, temperature profiles were calculated for an idealized tropospheric expansion of 30 hPa. These are shown in Figure 3, with the modern temperature profile with and without a 30 hPa offset included for reference. The change in the height and temperature of the cold point tropopause for profiles with modified ozone relative to the shifted profiles is listed to emphasize the changes to the temperature structure of the TTL.

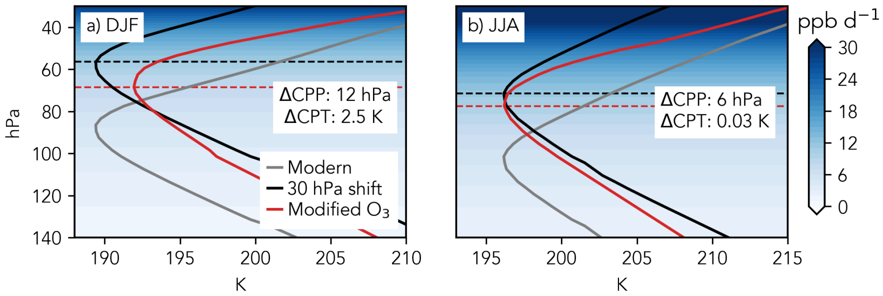

Figure 3. The upward shift of the cold point tropopause is limited in profiles that include ozone production (red) relative to those that are purely shifted upwards (black). Ozone production is shown in the blue shading, and the changes in cold point tropopause pressure and height relative to the "30 hPa shift" profiles are included to highlight the thermodynamic impact of this effect.

The temperature profiles in Figure 3 show that the upward shift of the cold point tropopause is limited by its movement up the ozone production gradient. In DJF, this compression is 40% of the 30 hPa expansion, while in JJA the effect is 20% of the rate tropospheric expansion. This decreases the extent of subadiabatic cooling between the top of the troposphere and the cold point tropopause, which combines with increased local radiative heating to increase the cold point tropopause temperature by 2.5 K in boreal winter and 0.03 K in boreal summer. Given that the cold point tropopause is at higher altitudes in DJF today, this difference between the seasons is not surprising – ozone production increases non-linearly with height, so tropospheric expansion will have a greater impact on local ozone production when the tropopause is higher to start with.

These increases in the cold point tropopause temperature and decreases in pressure increase the water vapor concentration at the cold point tropopause by 1.3 and 1.2 ppmv for the DJF and JJA "Modified O_3" temperature profiles relative to their respective "Modern" temperature profiles. These are significant increases relative to the modern annual mean lower stratospheric water vapor concentration of about 4 ppmv and would lead to an increase in water vapor throughout the stratosphere.

4.3 Effects of enhanced upwelling

In state-of-the art climate models, the Brewer-Dobson circulation – as quantified by the upward mass flux at 70 hPa – accelerates by 7 to 10% per degree of surface warming (Abalos et al., 2021), although this signal could be due to the upwelling profile following the tropopause upwards (Oberländer-Hayn et al., 2016). Enhanced upwelling would lessen the sharpening of the ozone gradient shown in Figure 2 by decreasing the transit time of air from its ozone-poor origin to the cold point tropopause, and it would increase dynamic cooling throughout the TTL, thereby decreasing the cold point tropopause temperature. Both of these effects could negate the results discussed above, so the analysis is repeated here with a range of vertical velocity accelerations to determine the robustness of the production mechanism.

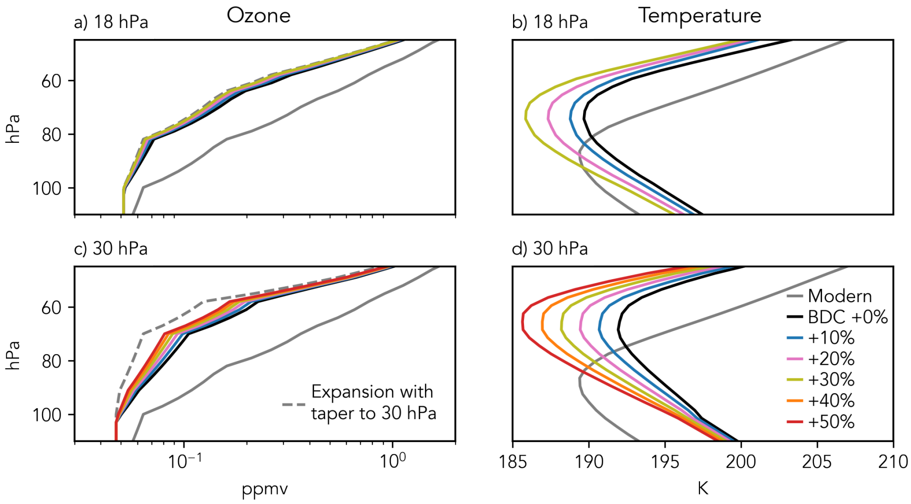

Figure 4. The effects of enhanced upwelling on lower stratospheric ozone (a and c) and temperature (b and d) profiles in DJF following 18 hPa (top row) and 30 hPa (bottom row) of tropospheric expansion. Details of the modified ozone profiles and radiative transfer calculations are described in the text, and corresponding profiles for JJA are shown in Figure S4.

To create ozone profiles that emulate enhanced upwelling in the TTL and lower stratosphere, the method used in Section 4.1 is modified with shorter timesteps; i.e. the path of air to the cold point tropopause is assumed to be the same, but the ozone production at each location is reduced because the air traverses the levels more quickly. As shown in the left column of Figure 4, ozone concentrations throughout the TTL and lower stratosphere decrease as the transit time to each level is decreased, which is consistent with recent work showing that stronger upwelling will advect ozone-poor air deeper into the stratosphere (Match & Gerber, 2022). For 18 hPa of tropospheric expansion, the increase in the ozone concentration at the cold point tropopause is small and is nearly eliminated by the increased rate of upwelling, while the effect of increased ozone production cannot be negated by enhanced upwelling following 30 hPa of expansion. In cold point-relative coordinates, lower stratospheric ozone increases when ozone production dominates over increased upwelling rates.

Temperature profiles were then calculated with these ozone profiles and dynamic cooling rates amplified in proportion to the increased upwelling rates. As shown in the right column of Figure 4, enhanced upwelling quickly dominates over the effect of increased ozone production following 18 hPa of tropospheric expansion, while the change in cold point tropopause temperature remains positive in DJF following 30 hPa of expansion when the acceleration is less than 30%. Given that all analysis done here includes a vertical shift of the upwelling profile, the upward flux at a fixed pressure level of 70 hPa required to overcome the effect of increased ozone production on the cold point tropopause could be outside of the range of model projections.

5 Discussion and Summary

5.1 Implications for recent observations

The ozone budget analysis performed here presents a mechanism for lower stratospheric ozone to increase following tropospheric expansion, which can help explain the persistence of lower stratospheric ozone concentrations in recent decades despite an expected decrease (Thompson et al., 2021). This mechanism's foundation is the strength of the ozone production gradient in the lower stratosphere: photochemical ozone production is insensitive to the height of the tropopause, so moving the tropopause and lower stratosphere up in altitude will push them into a region with a larger ozone source.

If the Brewer-Dobson circulation accelerated over the past two decades, then an increase in the ozone production rate in the tropical lower stratosphere may have compensated for the decreased transit time of air ascending from the troposphere and extratropical lower stratosphere. This would have maintained the local balance of transport and production and held ozone concentrations constant when measured in tropopause-following coordinates. Given that changes in ozone production near the tropopause are small for small rates of tropospheric expansion in the current climate, the apparent balancing of transport and production following surface warming suggests that the Brewer-Dobson circulation must not have accelerated significantly in the past two decades, agreeing with previous literature (Fu et al., 2019; Diallo et al., 2021). It is also possible that upwelling rates may have also been shifted upwards by tropospheric expansion and have not strengthened relative to the tropopause (Oberländer-Hayn et al., 2016).

5.2 Implications for future projections

In a region where ozone concentrations are determined by the balance of production and the transport of ozone-poor air, different mechanisms can dominate depending on the height of the tropopause and the strength of the Brewer-Dobson circulation. Match and Gerber (2022) showed that enhanced transport of ozone-poor air from the troposphere can decrease lower stratospheric ozone concentrations even when using tropopause-following coordinates. The work presented here does not refute those findings – if the effects of enhanced upwelling were to dominate over increased production rates, ozone concentrations above the tropical tropopause would decrease due to the decrease in ozone production as air ascends to the lower stratosphere. Changes to ozone production above the tropopause may be small in the near future, but as the troposphere continues to warm and the tropopause moves further up the ozone production gradient, TTL and lower stratospheric ozone concentrations will increase when measured relative to the tropopause.

This leads ozone concentrations to act as a radiative cap on the upward excursion of the cold point tropopause: when the LZRH is shifted up by 30 hPa, the cold point tropopause only shifts up by 18 hPa in boreal winter and 24 hPa in boreal summer, thereby limiting the amount of subadiabatic cooling that can occur between the two levels. The compression of the layer betweeen the LZRH and the cold point tropopause is consistent with the findings of Lin et al. (2017), who showed that the LZRH and lapse rate tropopause both rise more than the cold point tropopause in a model with sea surface temperatures increased by 4 K. That work also noted an increase in lower stratospheric ozone and temperature when using tropopause-following coordinates, which can be explained by the shift of the tropopause up the ozone production gradient described here.

In this study, ozone production above the LZRH is shown to increase the cold point tropopause temperature by about 2.5 K in boreal winter and 0.03 K in boreal summer following 5 K of surface warming and 30 hPa of tropospheric expansion without an increase in upwelling velocity at the cold point tropopause. This will increase of water vapor concentrations of air entering the stratosphere by greater than 1 ppmv, which would result in a positive climate feedback with a radiative forcing of about 0.25 W m^{-2} (Solomon et al., 2010). Additionally, this increase in stratospheric water vapor would increase the availability of hydrogen oxide radicals, which catalyze ozone destruction at low latitudes (Dvortsov & Solomon, 2001), and contribute to high latitude ozone destruction by allowing chlorine activation to occur at higher temperatures (Drdla & Müller, 2012).

Finally, this work highlights the need for high vertical resolution data for studies of TTL and lower stratospheric composition and thermodynamics. In both models and observations, tropopause-following coordinates cannot be used if tropospheric expansion cannot be resolved. Temperature and ozone measurements taken at constant heights will not reveal subtle shifts in the cold point tropopause, which would mask the mechanism presented here as the surface warms. This can lead to spurious trends in local temperature and ozone concentration and disagreement between models and observations with differing vertical grids.

6 Open Research

SWOOSH ozone data can be accessed through NOAA's Chemical Sciences Laboratory (`https://csl.noaa.gov/groups/csl8/swoosh/`), ERA5 temperature and wind data can be accessed through Copernicus Climate Change Service (`https://apps.ecmwf.int/data-catalogues/era5/?type=an&class=ea&stream=oper&expver=1`), and Radio Occultation data can be accessed through the ROM SAF Product Archive (`https://www.romsaf.org/product\_archive.php`; registration required). WACCM ozone production rates for 2004 to 2009 were supplied by Marta Abalos by email (mabalosa@ucm.es). LAGRANTO trajectory data, future WACCM ozone production rates, and code to produce figures are available on Zenodo (`https://doi.org/10.5281/zenodo.8219306` (Bourguet, 2023)). The Python interface for RRTMG was supplied through Konrad, which is available at `https://github.com/atmtools/konrad/blob/main/README.md`.

Acknowledgments
Thanks to Marianna Linz and Aaron Match for helpful conversations and feedback.

References

Abalos, M., Calvo, N., Benito-Barca, S., Garny, H., Hardiman, S. C., Lin, P., ... Yoshida, K. (2021). The brewer–dobson circulation in cmip6. *Atmospheric Chemistry and Physics*, *21*(17), 13571–13591. Retrieved from `https://acp.copernicus.org/articles/21/13571/2021/` doi: 10.5194/acp-21-13571-2021

Abalos, M., Randel, W., Kinnison, D., & Serrano, E. (2013). Quantifying tracer transport in the tropical lower stratosphere using waccm. *Atmospheric Chemistry and Physics*, *13*(21), 10591–10607. doi: 10.5194/acp-13-10591-2013

Abalos, M., Randel, W. J., Kinnison, D. E., & Garcia, R. R. (2017). Using the artificial tracer e90 to examine present and future utls tracer transport in waccm. *Journal of the Atmospheric Sciences*, *74*(10), 3383–3403. doi: 10.1175/JAS-D-17-0135.1

Ball, W. T., Chiodo, G., Abalos, M., Alsing, J., & Stenke, A. (2020). Inconsistencies between chemistry–climate models and observed lower stratospheric ozone trends since 1998. *Atmospheric Chemistry and Physics*, *20*(16), 9737–9752. Retrieved from `https://acp.copernicus.org/articles/20/9737/2020/` doi: 10.5194/acp-20-9737-2020

Birner, T., & Charlesworth, E. J. (2017). On the relative importance of radiative and dynamical heating for tropical tropopause temperatures. *Journal of Geophysical Research: Atmospheres*, *122*(13), 6782–6797. doi: 10.1002/2016JD026445

Bourguet, S. (2023, August). *The Impact of Ozone Production on Future Cold Point Tropopause Warming and Expansion.* Zenodo. Retrieved from https://doi.org/10.5281/zenodo.8219306 doi: 10.5281/zenodo.8219306

Bourguet, S., & Linz, M. (2022). The impact of improved spatial and temporal resolution of reanalysis data on lagrangian studies of the tropical tropopause layer. *Atmospheric Chemistry and Physics*, *22*(20), 13325–13339. Retrieved from https://acp.copernicus.org/articles/22/13325/2022/ doi: 10.5194/acp-22-13325-2022

Brewer, A. W. (1949). Evidence for a world circulation provided by the measurements of helium and water vapour distribution in the stratosphere. *Quarterly Journal of the Royal Meteorological Society*, *75*(326), 351–363. doi: 10.1002/qj.49707532603

Chiodo, G., Polvani, L. M., Marsh, D. R., Ball, W., Muthers, S., Stenke, A., ... Tsigaridis, K. (2018). The ozone response to quadrupled co2 concentrations. *J. Climate*, *31*(10), 3893–3907. doi: 10.1175/JCLI-D-17-0492.1

Davis, S. M., Rosenlof, K. H., Hassler, B., Hurst, D. F., Read, W. G., Vömel, H., ... Damadeo, R. (2016). The stratospheric water and ozone satellite homogenized (swoosh) database: a long-term database for climate studies. *Earth system science data*, *8*(2), 461–490. doi: 10.5194/essd-8-461-2016

Diallo, M., Ern, M., & Ploeger, F. (2021). The advective brewer–dobson circulation in the era5 reanalysis: climatology, variability, and trends. *Atmospheric Chemistry and Physics*, *21*(10), 7515–7544. Retrieved from https://acp.copernicus.org/articles/21/7515/2021/ doi: 10.5194/acp-21-7515-2021

Drdla, K., & Müller, R. (2012). Temperature thresholds for chlorine activation and ozone loss in the polar stratosphere. *Annales Geophysicae*, *30*(7), 1055–1073. Retrieved from https://angeo.copernicus.org/articles/30/1055/2012/ doi: 10.5194/angeo-30-1055-2012

Dvortsov, V. L., & Solomon, S. (2001). Response of the stratospheric temperatures and ozone to past and future increases in stratospheric humidity. *Journal of Geophysical Research: Atmospheres*, *106*(D7), 7505–7514. doi: 10.1029/2000JD900637

Eyring, V., Shepherd, T. G., & Waugh, D. W. (Eds.). (2010). *SPARC CCMVal Report on the Evaluation of Chemistry-Climate Models* (Vol. No. 5; Tech. Rep.). SPARC. Retrieved from http://www.sparc-climate.org/publications/sparc-reports/

Fu, Q., Solomon, S., Pahlavan, H. A., & Lin, P. (2019, nov). Observed changes in brewer–dobson circulation for 1980–2018. *Environmental Research Letters*, *14*(11), 114026. Retrieved from https://dx.doi.org/10.1088/1748-9326/ab4de7 doi: 10.1088/1748-9326/ab4de7

Gettelman, A., Birner, T., Eyring, V., Akiyoshi, H., Bekki, S., Brühl, C., ... Tian, W. (2009). The tropical tropopause layer 1960–2100. *Atmospheric Chemistry and Physics*, *9*(5), 1621–1637. Retrieved from https://acp.copernicus.org/articles/9/1621/2009/ doi: 10.5194/acp-9-1621-2009

Gettelman, A., Hegglin, M. I., Son, S.-W., Kim, J., Fujiwara, M., Birner, T., ... others (2010). Multimodel assessment of the upper troposphere and lower stratosphere: Tropics and global trends. *Journal of Geophysical Research: Atmospheres*, *115*(D3). doi: 10.1029/2009JD013638

Gleisner, H., Lauritsen, K. B., Nielsen, J. K., & Syndergaard, S. (2020). Evaluation of the 15-year rom saf monthly mean gps radio occultation climate data record. *Atmospheric Measurement Techniques*, *13*(6), 3081–3098. doi: 10.5194/amt-13-3081-2020

Grise, K. M., Thompson, D. W. J., & Birner, T. (2010). A global survey of static stability in the stratosphere and upper troposphere. *Journal of Climate*, *23*(9), 2275 - 2292. Retrieved from https://journals.ametsoc.org/view/

journals/clim/23/9/2009jcli3369.1.xml doi: https://doi.org/10.1175/2009JCLI3369.1

Hersbach, H., Bell, B., Berrisford, P., Hirahara, S., Horányi, A., Muñoz-Sabater, J., … Thépaut, J.-N. (2020). The era5 global reanalysis. *Quarterly Journal of the Royal Meteorological Society*, *146*(730), 1999–2049. Retrieved from https://rmets.onlinelibrary.wiley.com/doi/abs/10.1002/qj.3803 doi: 10.1002/qj.3803

Ho, S.-p., Hunt, D., Steiner, A. K., Mannucci, A. J., Kirchengast, G., Gleisner, H., … others (2012). Reproducibility of gps radio occultation data for climate monitoring: Profile-to-profile inter-comparison of champ climate records 2002 to 2008 from six data centers. *Journal of Geophysical Research: Atmospheres*, *117*(D18). doi: 10.1029/2012JD017665

Jonsson, A. I., de Grandpré, J., Fomichev, V. I., McConnell, J. C., & Beagley, S. R. (2004). Doubled co2-induced cooling in the middle atmosphere: Photochemical analysis of the ozone radiative feedback. *Journal of Geophysical Research: Atmospheres*, *109*(D24). Retrieved from https://agupubs.onlinelibrary.wiley.com/doi/abs/10.1029/2004JD005093 doi: https://doi.org/10.1029/2004JD005093

Keeble, J., Hassler, B., Banerjee, A., Checa-Garcia, R., Chiodo, G., Davis, S., … others (2021). Evaluating stratospheric ozone and water vapour changes in cmip6 models from 1850 to 2100. *Atmospheric Chemistry and Physics*, *21*(6), 5015–5061. doi: 10.5194/acp-21-5015-2021

Kluft, L., Dacie, S., Buehler, S. A., Schmidt, H., & Stevens, B. (2019). Re-examining the first climate models: Climate sensitivity of a modern radiative–convective equilibrium model. *Journal of Climate*, *32*(23), 8111–8125. doi: 10.1175/JCLI-D-18-0774.1

Lin, P., Paynter, D., Ming, Y., & Ramaswamy, V. (2017). Changes of the tropical tropopause layer under global warming. *Journal of Climate*, *30*(4), 1245–1258. doi: 10.1175/JCLI-D-16-0457.1

Match, A., & Fueglistaler, S. (2021). Large internal variability dominates over global warming signal in observed lower stratospheric qbo amplitude. *Journal of Climate*, *34*(24), 9823–9836. doi: 10.1175/JCLI-D-21-0270.1

Match, A., & Gerber, E. P. (2022). Tropospheric expansion under global warming reduces tropical lower stratospheric ozone. *Geophysical Research Letters*, *49*(19), e2022GL099463. doi: 10.1029/2022GL099463

Ming, A., Hitchcock, P., & Haynes, P. (2016). The double peak in upwelling and heating in the tropical lower stratosphere. *Journal of the Atmospheric Sciences*, *73*(5), 1889–1901. doi: 10.1175/JAS-D-15-0293.1

Mlawer, E. J., Taubman, S. J., Brown, P. D., Iacono, M. J., & Clough, S. A. (1997). Radiative transfer for inhomogeneous atmospheres: Rrtm, a validated correlated-k model for the longwave. *Journal of Geophysical Research: Atmospheres*, *102*(D14), 16663–16682. doi: 10.1029/97JD00237

Oberländer-Hayn, S., Gerber, E. P., Abalichin, J., Akiyoshi, H., Kerschbaumer, A., Kubin, A., … Oman, L. D. (2016). Is the brewer-dobson circulation increasing or moving upward? *Geophysical Research Letters*, *43*(4), 1772-1779. Retrieved from https://agupubs.onlinelibrary.wiley.com/doi/abs/10.1002/2015GL067545 doi: 10.1002/2015GL067545

Perliski, L. M., Solomon, S., & London, J. (1989). On the interpretation of seasonal variations of stratospheric ozone. *Planetary and Space Science*, *37*(12), 1527–1538. doi: 10.1016/0032-0633(89)90143-8

Randel, W. J., Park, M., Wu, F., & Livesey, N. (2007). A large annual cycle in ozone above the tropical tropopause linked to the brewer–dobson circulation. *Journal of the Atmospheric Sciences*, *64*(12), 4479 - 4488. Retrieved from https://journals.ametsoc.org/view/journals/atsc/64/12/2007jas2409.1.xml doi: 10.1175/2007JAS2409.1

Shepherd, T. G. (2008). Dynamics, stratospheric ozone, and climate change. *Atmosphere-Ocean*, *46*(1), 117–138. doi: 10.3137/ao.460106

Solomon, S., Rosenlof, K. H., Portmann, R. W., Daniel, J. S., Davis, S. M., Sanford, T. J., & Plattner, G.-K. (2010). Contributions of stratospheric water vapor to decadal changes in the rate of global warming. *Science*, *327*(5970), 1219-1223. Retrieved from `https://www.science.org/doi/abs/10.1126/science.1182488` doi: 10.1126/science.1182488

Sprenger, M., & Wernli, H. (2015). The lagranto lagrangian analysis tool – version 2.0. *Geoscientific Model Development*, *8*(8), 2569–2586. Retrieved from `https://gmd.copernicus.org/articles/8/2569/2015/` doi: 10.5194/gmd-8-2569-2015

Steiner, A., Hunt, D., Ho, S.-P., Kirchengast, G., Mannucci, A., Scherllin-Pirscher, B., ... others (2013). Quantification of structural uncertainty in climate data records from gps radio occultation. *Atmospheric Chemistry and Physics*, *13*(3), 1469–1484. doi: 10.5194/acp-13-1469-2013

Thompson, A. M., Stauffer, R. M., Wargan, K., Witte, J. C., Kollonige, D. E., & Ziemke, J. R. (2021). Regional and seasonal trends in tropical ozone from shadoz profiles: Reference for models and satellite products. *Journal of Geophysical Research: Atmospheres*, *126*(22), e2021JD034691. Retrieved from `https://agupubs.onlinelibrary.wiley.com/doi/abs/10.1029/2021JD034691` (e2021JD034691 2021JD034691) doi: 10.1029/2021JD034691

Wild, O. (2007). Modelling the global tropospheric ozone budget: exploring the variability in current models. *Atmospheric Chemistry and Physics*, *7*(10), 2643–2660. Retrieved from `https://acp.copernicus.org/articles/7/2643/2007/` doi: 10.5194/acp-7-2643-2007

The Impact of Ozone Production on Future Cold Point Tropopause Warming and Expansion

Stephen Bourguet

[1]Harvard University, Department of Earth and Planetary Sciences, Harvard University, Cambridge, MA 02138, USA

Key Points:

- Ozone concentrations at the cold point tropopause and above 30 hPa in the tropics are approximately constant throughout the year.
- At the cold point tropopause, this concentration is determined by the origin of air and in-situ ozone production.
- Increases to the cold point tropopause height will increase local ozone production, inducing local warming and limiting further expansion.

Corresponding author: Stephen Bourguet, `Stephen_Bourguet@g.harvard.edu`

Abstract

A robust thermodynamic response of increased greenhouse gas forcing is an expansion of the troposphere, which may decrease ozone concentrations in the lower stratosphere and warm the tropopause. Yet, observations of lower stratospheric ozone do not agree with model projections, and the net effect of greenhouse gas forcing on the temperature structure of the region between the tropical troposphere and stratosphere is unclear. Here, I isolate the role of local ozone production in setting the height of the cold point tropopause and the ozone concentrations above this level. Increased ozone production near the tropopause following tropospheric expansion will sharpen the vertical ozone gradient of the lower stratosphere and decrease the distance between the top of the troposphere and the cold point tropopause. This would suppress tropospheric expansion and increase the water vapor concentration of the stratosphere, which amplifies global warming and contributes to stratospheric ozone destruction.

Plain Language Summary

As greenhouse gas emissions warm the earth's surface, the lowermost layer of the atmosphere will expand upwards and the middle atmosphere will cool and shrink. The effect of these changes on the ozone and temperature profiles of the region that bridges the lower and middle atmosphere has been studied previously, but there is still some debate on how these profiles will evolve. Here, I show how ozone production, which does not depend on the height of atmospheric layers, will increase within this transition region, thereby increasing its ozone concentration. This helps explain discrepancies between model projections of ozone concentrations and observations. Additionally, increased ozone concentrations will increase the temperature of air entering the stratosphere, which allows this air to hold more water vapor and has important implications for atmospheric chemistry and global warming.

1 Introduction

Tropical lower stratospheric ozone concentrations are projected to decrease following surface warming (Eyring et al., 2010), but observed decreases over the past two decades are insignificant when considering changes to tropopause height (Thompson et al., 2021). This is part of broader disagreement between ozone projections in chemistry-climate models and observations which needs to be reconciled in order to understand the recovery of the protective stratospheric ozone layer following the Montreal Protocol's global ban on halogen-containing ozone depleting substances in the late 1990s (Ball et al., 2020).

The ozone profile between the tropical tropopause and the lower stratosphere also influences atmospheric circulation and chemistry and surface climate (Ming et al., 2016). Near the tropical tropopause, ozone is a strong absorber of longwave radiation, and the temperature structure of the tropical tropopause layer (TTL) is sensitive to ozone concentrations therein (Birner & Charlesworth, 2017). This contributes to the strong static stability of the tropopause inversion layer and the lower stratosphere (Grise et al., 2010), as well as the extreme cold temperatures of the TTL which dehydrate air as it fills the stratosphere (Brewer, 1949). Water vapor impacts ozone chemistry and is a strong greenhouse gas near the tropopause (Dvortsov & Solomon, 2001; Solomon et al., 2010), and climate models project an increase in lower stratospheric water vapor with surface warming (Gettelman et al., 2010; Keeble et al., 2021). Yet, these models cannot reproduce observations, and ozone concentrations have been identified as a driver of intermodel disagreement (Gettelman et al., 2009).

The response of lower stratospheric ozone to greenhouse gas forcing is complex. Tropospheric expansion, which is a robust thermodynamic consequence of surface warming, will not simply shift the stratospheric ozone profile upwards by the extent that the tropopause is displaced. Instead, the lower stratospheric ozone profile will be pushed upwards, while ozone concentrations in regions dominated by photochemistry will be unaffected by the transport of ozone-poor air from below (Perliski et al., 1989). In the absence of changes to upwelling or production, tropopause-following coordinates would eliminate any changes to lower stratospheric ozone, while an accelerated Brewer-Dobson circulation would enhance the transport of ozone-poor air into the stratosphere and decrease ozone concentrations in the region above the tropopause (Match & Gerber, 2022). On the other hand, changes to the ozone production rate could increase ozone concentrations in this region where the transport of ozone-poor air is balanced by local ozone production. Although ozone production in the lower stratosphere is weak, it strengthens rapidly with height, so the ozone concentration at the tropopause should be sensitive to its height.

Here, I explore how changes to ozone production following tropospheric expansion above the level of zero radiative heating (LZRH) could impact ozone concentrations in this region and alter the thermodynamic environment of the TTL. I do so by first establishing a budget for the ozone concentration at the cold point tropopause. I then construct ozone profiles that follow from tropospheric expansion with this budget and use a radiative transfer code to calculate corresponding changes to TTL temperatures and water vapor concentrations. Finally, I test the robustness of this mechanism to changes in tropical stratospheric upwelling.

2 Data and Methods

2.1 Ozone Data

Monthly-mean zonal-mean ozone profiles from the Stratospheric Water and OzOne Satellite Homogenized data set (SWOOSH, Davis et al. (2016)) were used to construct an ozone budget for the cold point tropopause. These data are on a pressure grid with two levels near the cold point tropopause (100 hPa and 82.5 hPa), so the ozone concentrations were interpolated to the cold point tropopause height diagnosed from monthly mean temperatures from the European Center for Medium-range Weather Forecasts latest reanalysis product, ERA5 (Hersbach et al., 2020), and the Radio Occultation Meteorology Satellite Application Facility's multi-mission data set (Ho et al., 2012; Steiner et al., 2013; Gleisner et al., 2020). This was done for 2002 to 2016, which are the years that all datasets were available.

Ozone production rates were taken from the Community Earth Systems Model's Whole Atmosphere Chemistry and Composition Model (CESM1 WACCM4). For the base state, an average over 2004 to 2009 was used (data are described in Abalos et al. (2013)). For two surface warming scenarios, uniform temperature increases of 3 and 5 K were imposed with CO_2 concentrations of 560 and 1000 ppm, respectively. Zonal mean ozone production for each of these scenarios is shown in Figure S1.

2.2 The Lagrangian Framework

Ozone concentrations within the TTL balance the advection of ozone-poor air from the troposphere with in-mixing of ozone-rich air from the extratropical lower stratosphere and in-situ photochemical production (Abalos et al., 2013). Therefore, the Lagrangian trajectory model LAGRANTO (Sprenger & Wernli, 2015) was used to trace the origin of air masses that ascend to the cold point tropopause and the path they take to calculate the cold point tropopause's ozone budget. Following the procedure of Bourguet and Linz (2022), reverse trajectories were initialized from 20°S to 20°N at all longitudes with 0.5° spacing on the last day of February and the last day of August in 2007, 2008, and 2009 near the cold point tropopause (90 hPa in boreal winter and 100 hPa in boreal summer). ERA5 hourly winds were used and trajectories were traced backwards for 90 days.

Using trajectory distributions, I construct the following budget for the cold point tropopause's ozone concentration:

$$O3_{c.p.} = O3_{initial} + \text{Net Production} + \text{Residual Mixing}. \tag{1}$$

The "initial" ozone concentration ($O3_{initial}$) depends on the timescale of interest – here, this is the average ozone concentration at the trajectories' locations at the end of integration (90 days prior to reaching the cold point tropopause). This was calculated using a weighted average of SWOOSH ozone concentrations, with the weighting determined by trajectory distributions. The net production term was calculated using trajectory weightings at the end of each day, with the net ozone production field taken from WACCM's zonal mean net ozone tendency.

"Residual" or sub-grid scale mixing can be diagnosed with this framework by comparing the observed cold point tropopause ozone concentration to the concentration calculated by Eq. 1 without mixing. To do so, ozone concentrations were initialized based on trajectory distributions 90 days prior to reaching the cold point tropopause and then increased each day according to the trajectories' average ozone tendency. Disagreement between the constructed ozone concentration at the end of the timeseries (the end of February or August) and the observed ozone concentrations were assumed to be caused by mixing that the Lagrangian framework cannot capture. In 2007, 2008, and 2009 respectively, the residual mixing terms were –3%, –8%, and –4% of the cold point tropopause's ozone concentration in February and 2%, —1%, and 14% in August. Thus, Eq. 1 can be reduced to:

$$O3_{c.p.} \approx O3_{initial} + \text{Net Production}. \tag{2}$$

2.3 Idealized Tropospheric Expansion

The following experiments are idealized representations of 3 and 5 K of surface warming, which would drive approximately 18 and 30 hPa of tropospheric expansion, respectively (Match & Fueglistaler, 2021). The results shown in the text are for 5 K of warming; corresponding plots for 3 K are shown in the supplemental.

2.3.1 Changes to Ozone at the Cold Point Tropopause

To calculate how ozone concentrations at the cold point tropopause will change with surface warming, it was assumed that in-mixing from the extratropics follows the tropopause upwards. Anticipated increases in the meridional ozone gradient (Shepherd, 2008) and mixing rates (Abalos et al., 2017) would increase the in-mixing of ozone, thereby making this a conservative treatment of future in-mixing. Tropospheric ozone concentrations were also assumed to remain negligible, which is reasonable given the lifetime of ozone in the troposphere (Wild, 2007). These assumptions simplify the time derivative of Eq. 2 to:

$$\Delta O3_{c.p.} = \Delta\text{Net Production}. \tag{3}$$

Trajectory distributions from 2008 with their pressure offset by the rate of tropospheric expansion were used to calculate ΔNet Production. This assumes that the path of air en route to the cold point tropopause will follow the tropopause upwards, which is consistent with the assumption of constant in-mixing from the extratropics. As discussed in Sections 2.1, the future zonal mean net ozone production rates are calculated using WACCM.

2.3.2 Temperature and Water Vapor

The radiative transfer code RRTMG (Mlawer et al., 1997; Kluft et al., 2019) with fixed dynamic heating was used to calculate how cold point tropopause pressures and temperatures will respond to changes in the ozone profiles following tropospheric expansion. To do so, the modified ozone profile was taken from Section 4.1, and the dynamic heating profile was shifted upwards according to the rate of tropospheric expansion. Temperatures beneath the LZRH were increased by 3 or 5 K, and the CO_2 concentrations were increased to 560 and 1000 ppm for the two experiments, respectively. Stratospheric water vapor concentrations were calculated based on Clausius-Clapeyron relationship at the cold point tropopause at each timestep. Additional details are given in Text S1.

3 Observed Cold Point Tropopause Ozone Concentrations

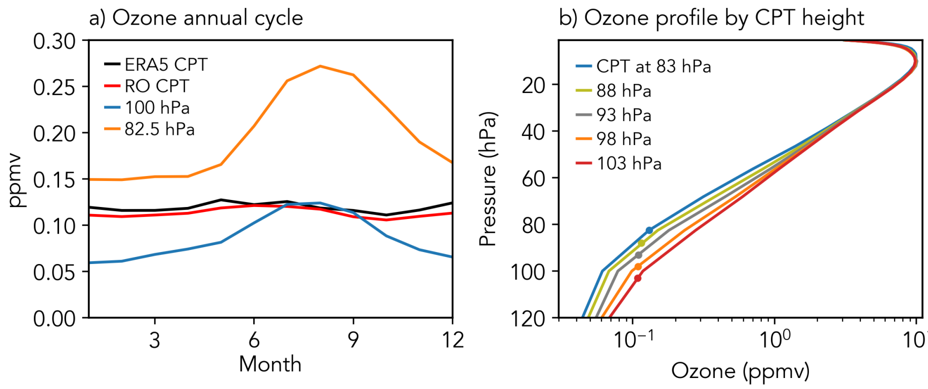

Figure 1. a) The annual cycle of zonal mean (15°S to 15°N) SWOOSH ozone concentrations at 100 hPa (blue line), 82.5 hPa (orange line), and the cold point tropopause interpolated from monthly mean radio occultations (red line) and ERA5 temperature profiles (black line). b) SWOOSH ozone profiles organized by ERA5 cold point tropopause height with the ozone concentration at the cold point tropopause marked with circles.

Figure 1a shows that the ozone concentration at the cold point tropopause is approximately constant throughout the year, while the concentrations at nearby pressure levels vary between the solstices. In the TTL, ozone concentrations at fixed heights will vary as the transport of ozone-poor air varies (Randel et al., 2007), leading to temperature changes that reinforce those already driven by variations in dynamic cooling (Birner & Charlesworth, 2017). The cold point tropopause is able to follow these changes to dynamic and radiative heating, resulting in its position on a fixed ozone surface.

SWOOSH ozone profiles are separated by the ERA5 cold point tropopause height in Figure 1b. These profiles emphasize the variance of lower stratospheric ozone concentrations as the cold point tropopause moves up and down in height. Ozone concentrations beneath 30 hPa covary with the movement of the cold point tropopause, while concentrations above 30 hPa are insensitive to lower stratospheric ozone variability. This reflects the division of stratospheric ozone into regimes of balanced transport and production in the lower to middle stratosphere and balanced production and loss in the middle to upper stratosphere (Perliski et al., 1989). Ozone concentrations at the cold point tropopause (highlighted by circles in Figure 1b) vary by less than 0.01 ppmv as the cold point tropopause height varies by 20 hPa.

These observations reveal a previously overlooked feature of the cold point tropopause in the modern climate: a fixed ozone concentration of about 0.12 ppmv. Given the seasonal and interannual fluctuations in the height of the cold point tropopause, this feature prompts the usage of cold point-relative coordinates to understand the ozone budget of the cold point tropopause and lowermost stratosphere.

4 Tropospheric Expansion

4.1 Ozone Profiles

To create ozone profiles that emulate the effect of 30 hPa of tropospheric expansion without increased ozone production beneath the cold point tropopause, ozone profiles were shifted up by 30 hPa and then tapered back to observations between the cold point tropopause and 30 hPa. This decreases ozone concentrations at fixed heights in the lower to middle stratosphere but does not change concentrations in tropopause-following coordinates. Ozone concentrations above 30 hPa were increased by 10% to simulate the decrease in odd-oxygen loss that would result from stratospheric cooling (Jonsson et al., 2004). (The increase aloft is not a result of tropospheric expansion but does impact TTL thermodynamics and ozone production by blocking shortwave radiation. Subsequent results are not sensitive to the choice of amplification within the range of model projections (Chiodo et al., 2018).)

To include increased ozone production between the LZRH and the cold point tropopause, the ozone concentration at the height 30 hPa above the modern cold point tropopause was calculated using Eq. 3. This would be the ozone concentration at the cold point tropopause if changes to its height were set by dynamics above the LZRH and not thermodynamics. Ozone concentrations were then increased from observations at the LZRH to this increased value at the lifted cold point tropopause.

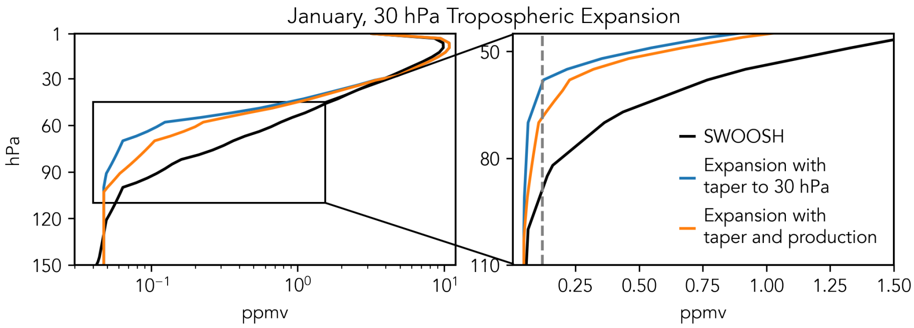

Figure 2. The 2002–2016 mean January ozone profile taken from SWOOSH (black line) and ozone profiles following 30 hPa of tropospheric expansion with and without increased ozone production (orange and blue, respectively). The 45 to 110 hPa layer is reproduced in the right panel to show the large difference near the cold point tropopause. The corresponding July ozone profile and profiles for 15 hPa of tropospheric expansion are shown in Figure S2.

The profiles for January following 30 hPa of tropospheric expansion are shown by the blue (expansion only) and orange (expansion and increased production) lines in Figure 2, with the modern ozone profile shown in black. By construction, these profiles are qualitatively similar to those in Figure 1b. In both cases, ozone varies with tropopause height in the region where transport and production are balanced, but the difference between the ozone profiles in Figure 2 comes from differences in production, rather than transport. In the right panel, which focuses on the TTL, a vertical line at the ozone concentration of the modern cold point tropopause (about 0.12 ppmv) is included to highlight where the cold point tropopause would be if it were to follow the same ozone concentration level as the troposphere expands.

4.2 Cold Point Tropopause Temperature and Water Vapor

Using the ozone profile shown in Figure 2 and the corresponding profile for JJA, temperature profiles were calculated for an idealized tropospheric expansion of 30 hPa. These are shown in Figure 3, with the modern temperature profile with and without a 30 hPa offset included for reference. The change in the height and temperature of the cold point tropopause for profiles with modified ozone relative to the shifted profiles is listed to emphasize the changes to the temperature structure of the TTL.

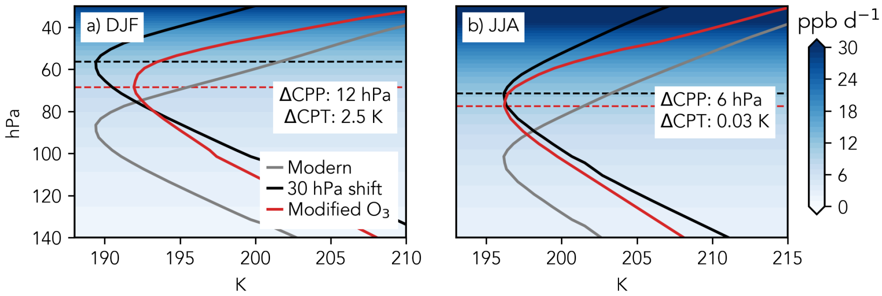

Figure 3. The upward shift of the cold point tropopause is limited in profiles that include ozone production (red) relative to those that are purely shifted upwards (black). Ozone production is shown in the blue shading, and the changes in cold point tropopause pressure and height relative to the "30 hPa shift" profiles are included to highlight the thermodynamic impact of this effect.

The temperature profiles in Figure 3 show that the upward shift of the cold point tropopause is limited by its movement up the ozone production gradient. In DJF, this compression is 40% of the 30 hPa expansion, while in JJA the effect is 20% of the rate tropospheric expansion. This decreases the extent of subadiabatic cooling between the top of the troposphere and the cold point tropopause, which combines with increased local radiative heating to increase the cold point tropopause temperature by 2.5 K in boreal winter and 0.03 K in boreal summer. Given that the cold point tropopause is at higher altitudes in DJF today, this difference between the seasons is not surprising – ozone production increases non-linearly with height, so tropospheric expansion will have a greater impact on local ozone production when the tropopause is higher to start with.

These increases in the cold point tropopause temperature and decreases in pressure increase the water vapor concentration at the cold point tropopause by 1.3 and 1.2 ppmv for the DJF and JJA "Modified O_3" temperature profiles relative to their respective "Modern" temperature profiles. These are significant increases relative to the modern annual mean lower stratospheric water vapor concentration of about 4 ppmv and would lead to an increase in water vapor throughout the stratosphere.

4.3 Effects of enhanced upwelling

In state-of-the art climate models, the Brewer-Dobson circulation – as quantified by the upward mass flux at 70 hPa – accelerates by 7 to 10% per degree of surface warming (Abalos et al., 2021), although this signal could be due to the upwelling profile following the tropopause upwards (Oberländer-Hayn et al., 2016). Enhanced upwelling would lessen the sharpening of the ozone gradient shown in Figure 2 by decreasing the transit time of air from its ozone-poor origin to the cold point tropopause, and it would increase dynamic cooling throughout the TTL, thereby decreasing the cold point tropopause temperature. Both of these effects could negate the results discussed above, so the analysis is repeated here with a range of vertical velocity accelerations to determine the robustness of the production mechanism.

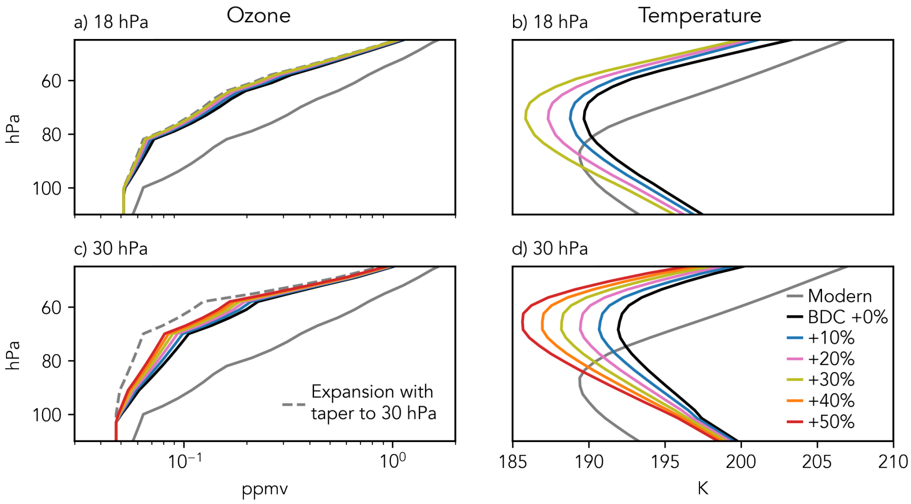

Figure 4. The effects of enhanced upwelling on lower stratospheric ozone (a and c) and temperature (b and d) profiles in DJF following 18 hPa (top row) and 30 hPa (bottom row) of tropospheric expansion. Details of the modified ozone profiles and radiative transfer calculations are described in the text, and corresponding profiles for JJA are shown in Figure S4.

To create ozone profiles that emulate enhanced upwelling in the TTL and lower stratosphere, the method used in Section 4.1 is modified with shorter timesteps; i.e. the path of air to the cold point tropopause is assumed to be the same, but the ozone production at each location is reduced because the air traverses the levels more quickly. As shown in the left column of Figure 4, ozone concentrations throughout the TTL and lower stratosphere decrease as the transit time to each level is decreased, which is consistent with recent work showing that stronger upwelling will advect ozone-poor air deeper into the stratosphere (Match & Gerber, 2022). For 18 hPa of tropospheric expansion, the increase in the ozone concentration at the cold point tropopause is small and is nearly eliminated by the increased rate of upwelling, while the effect of increased ozone production cannot be negated by enhanced upwelling following 30 hPa of expansion. In cold point-relative coordinates, lower stratospheric ozone increases when ozone production dominates over increased upwelling rates.

Temperature profiles were then calculated with these ozone profiles and dynamic cooling rates amplified in proportion to the increased upwelling rates. As shown in the right column of Figure 4, enhanced upwelling quickly dominates over the effect of increased ozone production following 18 hPa of tropospheric expansion, while the change in cold point tropopause temperature remains positive in DJF following 30 hPa of expansion when the acceleration is less than 30%. Given that all analysis done here includes a vertical shift of the upwelling profile, the upward flux at a fixed pressure level of 70 hPa required to overcome the effect of increased ozone production on the cold point tropopause could be outside of the range of model projections.

5 Discussion and Summary

5.1 Implications for recent observations

The ozone budget analysis performed here presents a mechanism for lower stratospheric ozone to increase following tropospheric expansion, which can help explain the persistence of lower stratospheric ozone concentrations in recent decades despite an expected decrease (Thompson et al., 2021). This mechanism's foundation is the strength of the ozone production gradient in the lower stratosphere: photochemical ozone production is insensitive to the height of the tropopause, so moving the tropopause and lower stratosphere up in altitude will push them into a region with a larger ozone source.

If the Brewer-Dobson circulation accelerated over the past two decades, then an increase in the ozone production rate in the tropical lower stratosphere may have compensated for the decreased transit time of air ascending from the troposphere and extratropical lower stratosphere. This would have maintained the local balance of transport and production and held ozone concentrations constant when measured in tropopause-following coordinates. Given that changes in ozone production near the tropopause are small for small rates of tropospheric expansion in the current climate, the apparent balancing of transport and production following surface warming suggests that the Brewer-Dobson circulation must not have accelerated significantly in the past two decades, agreeing with previous literature (Fu et al., 2019; Diallo et al., 2021). It is also possible that upwelling rates may have also been shifted upwards by tropospheric expansion and have not strengthened relative to the tropopause (Oberländer-Hayn et al., 2016).

5.2 Implications for future projections

In a region where ozone concentrations are determined by the balance of production and the transport of ozone-poor air, different mechanisms can dominate depending on the height of the tropopause and the strength of the Brewer-Dobson circulation. Match and Gerber (2022) showed that enhanced transport of ozone-poor air from the troposphere can decrease lower stratospheric ozone concentrations even when using tropopause-following coordinates. The work presented here does not refute those findings – if the effects of enhanced upwelling were to dominate over increased production rates, ozone concentrations above the tropical tropopause would decrease due to the decrease in ozone production as air ascends to the lower stratosphere. Changes to ozone production above the tropopause may be small in the near future, but as the troposphere continues to warm and the tropopause moves further up the ozone production gradient, TTL and lower stratospheric ozone concentrations will increase when measured relative to the tropopause.

This leads ozone concentrations to act as a radiative cap on the upward excursion of the cold point tropopause: when the LZRH is shifted up by 30 hPa, the cold point tropopause only shifts up by 18 hPa in boreal winter and 24 hPa in boreal summer, thereby limiting the amount of subadiabatic cooling that can occur between the two levels. The compression of the layer betweeen the LZRH and the cold point tropopause is consistent with the findings of Lin et al. (2017), who showed that the LZRH and lapse rate tropopause both rise more than the cold point tropopause in a model with sea surface temperatures increased by 4 K. That work also noted an increase in lower stratospheric ozone and temperature when using tropopause-following coordinates, which can be explained by the shift of the tropopause up the ozone production gradient described here.

In this study, ozone production above the LZRH is shown to increase the cold point tropopause temperature by about 2.5 K in boreal winter and 0.03 K in boreal summer following 5 K of surface warming and 30 hPa of tropospheric expansion without an increase in upwelling velocity at the cold point tropopause. This will increase of water vapor concentrations of air entering the stratosphere by greater than 1 ppmv, which would result in a positive climate feedback with a radiative forcing of about 0.25 W m^{-2} (Solomon et al., 2010). Additionally, this increase in stratospheric water vapor would increase the availability of hydrogen oxide radicals, which catalyze ozone destruction at low latitudes (Dvortsov & Solomon, 2001), and contribute to high latitude ozone destruction by allowing chlorine activation to occur at higher temperatures (Drdla & Müller, 2012).

Finally, this work highlights the need for high vertical resolution data for studies of TTL and lower stratospheric composition and thermodynamics. In both models and observations, tropopause-following coordinates cannot be used if tropospheric expansion cannot be resolved. Temperature and ozone measurements taken at constant heights will not reveal subtle shifts in the cold point tropopause, which would mask the mechanism presented here as the surface warms. This can lead to spurious trends in local temperature and ozone concentration and disagreement between models and observations with differing vertical grids.

6 Open Research

SWOOSH ozone data can be accessed through NOAA's Chemical Sciences Laboratory (`https://csl.noaa.gov/groups/csl8/swoosh/`), ERA5 temperature and wind data can be accessed through Copernicus Climate Change Service (`https://apps.ecmwf.int/data-catalogues/era5/?type=an&class=ea&stream=oper&expver=1`), and Radio Occultation data can be accessed through the ROM SAF Product Archive (`https://www.romsaf.org/product\_archive.php`; registration required). WACCM ozone production rates for 2004 to 2009 were supplied by Marta Abalos by email (mabalosa@ucm.es). LAGRANTO trajectory data, future WACCM ozone production rates, and code to produce figures are available on Zenodo (`https://doi.org/10.5281/zenodo.8219306` (Bourguet, 2023)). The Python interface for RRTMG was supplied through Konrad, which is available at `https://github.com/atmtools/konrad/blob/main/README.md`.

Acknowledgments

Thanks to Marianna Linz and Aaron Match for helpful conversations and feedback.

References

Abalos, M., Calvo, N., Benito-Barca, S., Garny, H., Hardiman, S. C., Lin, P., ... Yoshida, K. (2021). The brewer–dobson circulation in cmip6. *Atmospheric Chemistry and Physics*, *21*(17), 13571–13591. Retrieved from `https://acp.copernicus.org/articles/21/13571/2021/` doi: 10.5194/acp-21-13571-2021

Abalos, M., Randel, W., Kinnison, D., & Serrano, E. (2013). Quantifying tracer transport in the tropical lower stratosphere using waccm. *Atmospheric Chemistry and Physics*, *13*(21), 10591–10607. doi: 10.5194/acp-13-10591-2013

Abalos, M., Randel, W. J., Kinnison, D. E., & Garcia, R. R. (2017). Using the artificial tracer e90 to examine present and future utls tracer transport in waccm. *Journal of the Atmospheric Sciences*, *74*(10), 3383–3403. doi: 10.1175/JAS-D-17-0135.1

Ball, W. T., Chiodo, G., Abalos, M., Alsing, J., & Stenke, A. (2020). Inconsistencies between chemistry–climate models and observed lower stratospheric ozone trends since 1998. *Atmospheric Chemistry and Physics*, *20*(16), 9737–9752. Retrieved from `https://acp.copernicus.org/articles/20/9737/2020/` doi: 10.5194/acp-20-9737-2020

Birner, T., & Charlesworth, E. J. (2017). On the relative importance of radiative and dynamical heating for tropical tropopause temperatures. *Journal of Geophysical Research: Atmospheres*, *122*(13), 6782–6797. doi: 10.1002/2016JD026445

Bourguet, S. (2023, August). *The Impact of Ozone Production on Future Cold Point Tropopause Warming and Expansion.* Zenodo. Retrieved from https://doi.org/10.5281/zenodo.8219306 doi: 10.5281/zenodo.8219306

Bourguet, S., & Linz, M. (2022). The impact of improved spatial and temporal resolution of reanalysis data on lagrangian studies of the tropical tropopause layer. *Atmospheric Chemistry and Physics*, *22*(20), 13325–13339. Retrieved from https://acp.copernicus.org/articles/22/13325/2022/ doi: 10.5194/acp-22-13325-2022

Brewer, A. W. (1949). Evidence for a world circulation provided by the measurements of helium and water vapour distribution in the stratosphere. *Quarterly Journal of the Royal Meteorological Society*, *75*(326), 351–363. doi: 10.1002/qj.49707532603

Chiodo, G., Polvani, L. M., Marsh, D. R., Ball, W., Muthers, S., Stenke, A., ... Tsigaridis, K. (2018). The ozone response to quadrupled co2 concentrations. *J. Climate*, *31*(10), 3893–3907. doi: 10.1175/JCLI-D-17-0492.1

Davis, S. M., Rosenlof, K. H., Hassler, B., Hurst, D. F., Read, W. G., Vömel, H., ... Damadeo, R. (2016). The stratospheric water and ozone satellite homogenized (swoosh) database: a long-term database for climate studies. *Earth system science data*, *8*(2), 461–490. doi: 10.5194/essd-8-461-2016

Diallo, M., Ern, M., & Ploeger, F. (2021). The advective brewer–dobson circulation in the era5 reanalysis: climatology, variability, and trends. *Atmospheric Chemistry and Physics*, *21*(10), 7515–7544. Retrieved from https://acp.copernicus.org/articles/21/7515/2021/ doi: 10.5194/acp-21-7515-2021

Drdla, K., & Müller, R. (2012). Temperature thresholds for chlorine activation and ozone loss in the polar stratosphere. *Annales Geophysicae*, *30*(7), 1055–1073. Retrieved from https://angeo.copernicus.org/articles/30/1055/2012/ doi: 10.5194/angeo-30-1055-2012

Dvortsov, V. L., & Solomon, S. (2001). Response of the stratospheric temperatures and ozone to past and future increases in stratospheric humidity. *Journal of Geophysical Research: Atmospheres*, *106*(D7), 7505–7514. doi: 10.1029/2000JD900637

Eyring, V., Shepherd, T. G., & Waugh, D. W. (Eds.). (2010). *SPARC CCMVal Report on the Evaluation of Chemistry-Climate Models* (Vol. No. 5; Tech. Rep.). SPARC. Retrieved from http://www.sparc-climate.org/publications/sparc-reports/

Fu, Q., Solomon, S., Pahlavan, H. A., & Lin, P. (2019, nov). Observed changes in brewer–dobson circulation for 1980–2018. *Environmental Research Letters*, *14*(11), 114026. Retrieved from https://dx.doi.org/10.1088/1748-9326/ab4de7 doi: 10.1088/1748-9326/ab4de7

Gettelman, A., Birner, T., Eyring, V., Akiyoshi, H., Bekki, S., Brühl, C., ... Tian, W. (2009). The tropical tropopause layer 1960–2100. *Atmospheric Chemistry and Physics*, *9*(5), 1621–1637. Retrieved from https://acp.copernicus.org/articles/9/1621/2009/ doi: 10.5194/acp-9-1621-2009

Gettelman, A., Hegglin, M. I., Son, S.-W., Kim, J., Fujiwara, M., Birner, T., ... others (2010). Multimodel assessment of the upper troposphere and lower stratosphere: Tropics and global trends. *Journal of Geophysical Research: Atmospheres*, *115*(D3). doi: 10.1029/2009JD013638

Gleisner, H., Lauritsen, K. B., Nielsen, J. K., & Syndergaard, S. (2020). Evaluation of the 15-year rom saf monthly mean gps radio occultation climate data record. *Atmospheric Measurement Techniques*, *13*(6), 3081–3098. doi: 10.5194/amt-13-3081-2020

Grise, K. M., Thompson, D. W. J., & Birner, T. (2010). A global survey of static stability in the stratosphere and upper troposphere. *Journal of Climate*, *23*(9), 2275 - 2292. Retrieved from https://journals.ametsoc.org/view/

journals/clim/23/9/2009jcli3369.1.xml doi: https://doi.org/10.1175/2009JCLI3369.1

Hersbach, H., Bell, B., Berrisford, P., Hirahara, S., Horányi, A., Muñoz-Sabater, J., ... Thépaut, J.-N. (2020). The era5 global reanalysis. *Quarterly Journal of the Royal Meteorological Society*, *146*(730), 1999–2049. Retrieved from https://rmets.onlinelibrary.wiley.com/doi/abs/10.1002/qj.3803 doi: 10.1002/qj.3803

Ho, S.-p., Hunt, D., Steiner, A. K., Mannucci, A. J., Kirchengast, G., Gleisner, H., ... others (2012). Reproducibility of gps radio occultation data for climate monitoring: Profile-to-profile inter-comparison of champ climate records 2002 to 2008 from six data centers. *Journal of Geophysical Research: Atmospheres*, *117*(D18). doi: 10.1029/2012JD017665

Jonsson, A. I., de Grandpré, J., Fomichev, V. I., McConnell, J. C., & Beagley, S. R. (2004). Doubled co2-induced cooling in the middle atmosphere: Photochemical analysis of the ozone radiative feedback. *Journal of Geophysical Research: Atmospheres*, *109*(D24). Retrieved from https://agupubs.onlinelibrary.wiley.com/doi/abs/10.1029/2004JD005093 doi: https://doi.org/10.1029/2004JD005093

Keeble, J., Hassler, B., Banerjee, A., Checa-Garcia, R., Chiodo, G., Davis, S., ... others (2021). Evaluating stratospheric ozone and water vapour changes in cmip6 models from 1850 to 2100. *Atmospheric Chemistry and Physics*, *21*(6), 5015–5061. doi: 10.5194/acp-21-5015-2021

Kluft, L., Dacie, S., Buehler, S. A., Schmidt, H., & Stevens, B. (2019). Re-examining the first climate models: Climate sensitivity of a modern radiative–convective equilibrium model. *Journal of Climate*, *32*(23), 8111–8125. doi: 10.1175/JCLI-D-18-0774.1

Lin, P., Paynter, D., Ming, Y., & Ramaswamy, V. (2017). Changes of the tropical tropopause layer under global warming. *Journal of Climate*, *30*(4), 1245–1258. doi: 10.1175/JCLI-D-16-0457.1

Match, A., & Fueglistaler, S. (2021). Large internal variability dominates over global warming signal in observed lower stratospheric qbo amplitude. *Journal of Climate*, *34*(24), 9823–9836. doi: 10.1175/JCLI-D-21-0270.1

Match, A., & Gerber, E. P. (2022). Tropospheric expansion under global warming reduces tropical lower stratospheric ozone. *Geophysical Research Letters*, *49*(19), e2022GL099463. doi: 10.1029/2022GL099463

Ming, A., Hitchcock, P., & Haynes, P. (2016). The double peak in upwelling and heating in the tropical lower stratosphere. *Journal of the Atmospheric Sciences*, *73*(5), 1889–1901. doi: 10.1175/JAS-D-15-0293.1

Mlawer, E. J., Taubman, S. J., Brown, P. D., Iacono, M. J., & Clough, S. A. (1997). Radiative transfer for inhomogeneous atmospheres: Rrtm, a validated correlated-k model for the longwave. *Journal of Geophysical Research: Atmospheres*, *102*(D14), 16663–16682. doi: 10.1029/97JD00237

Oberländer-Hayn, S., Gerber, E. P., Abalichin, J., Akiyoshi, H., Kerschbaumer, A., Kubin, A., ... Oman, L. D. (2016). Is the brewer-dobson circulation increasing or moving upward? *Geophysical Research Letters*, *43*(4), 1772-1779. Retrieved from https://agupubs.onlinelibrary.wiley.com/doi/abs/10.1002/2015GL067545 doi: 10.1002/2015GL067545

Perliski, L. M., Solomon, S., & London, J. (1989). On the interpretation of seasonal variations of stratospheric ozone. *Planetary and Space Science*, *37*(12), 1527–1538. doi: 10.1016/0032-0633(89)90143-8

Randel, W. J., Park, M., Wu, F., & Livesey, N. (2007). A large annual cycle in ozone above the tropical tropopause linked to the brewer–dobson circulation. *Journal of the Atmospheric Sciences*, *64*(12), 4479 - 4488. Retrieved from https://journals.ametsoc.org/view/journals/atsc/64/12/2007jas2409.1.xml doi: 10.1175/2007JAS2409.1

Shepherd, T. G. (2008). Dynamics, stratospheric ozone, and climate change. *Atmosphere-Ocean*, *46*(1), 117–138. doi: 10.3137/ao.460106

Solomon, S., Rosenlof, K. H., Portmann, R. W., Daniel, J. S., Davis, S. M., Sanford, T. J., & Plattner, G.-K. (2010). Contributions of stratospheric water vapor to decadal changes in the rate of global warming. *Science*, *327*(5970), 1219-1223. Retrieved from `https://www.science.org/doi/abs/10.1126/science.1182488` doi: 10.1126/science.1182488

Sprenger, M., & Wernli, H. (2015). The lagranto lagrangian analysis tool – version 2.0. *Geoscientific Model Development*, *8*(8), 2569–2586. Retrieved from `https://gmd.copernicus.org/articles/8/2569/2015/` doi: 10.5194/gmd-8-2569-2015

Steiner, A., Hunt, D., Ho, S.-P., Kirchengast, G., Mannucci, A., Scherllin-Pirscher, B., ... others (2013). Quantification of structural uncertainty in climate data records from gps radio occultation. *Atmospheric Chemistry and Physics*, *13*(3), 1469–1484. doi: 10.5194/acp-13-1469-2013

Thompson, A. M., Stauffer, R. M., Wargan, K., Witte, J. C., Kollonige, D. E., & Ziemke, J. R. (2021). Regional and seasonal trends in tropical ozone from shadoz profiles: Reference for models and satellite products. *Journal of Geophysical Research: Atmospheres*, *126*(22), e2021JD034691. Retrieved from `https://agupubs.onlinelibrary.wiley.com/doi/abs/10.1029/2021JD034691` (e2021JD034691 2021JD034691) doi: 10.1029/2021JD034691

Wild, O. (2007). Modelling the global tropospheric ozone budget: exploring the variability in current models. *Atmospheric Chemistry and Physics*, *7*(10), 2643–2660. Retrieved from `https://acp.copernicus.org/articles/7/2643/2007/` doi: 10.5194/acp-7-2643-2007

Supporting Information for "The Impact of Ozone Production on Future Cold Point Tropopause Warming and Expansion"

Stephen Bourguet[1]

[1]Harvard University, Department of Earth and Planetary Sciences, 20 Oxford Street, Cambridge, MA 02138

Contents of this file

Text S1. Radiative transfer code set-up

The dynamic heating profile above the level of zero radiative heating (LZRH) was taken from the radiative disequilibrium of the ERA5 zonal mean temperatures and was tapered back to observations at 30 hPa to keep the dynamic cooling of deep branch of the BDC fixed, and the water vapor profile in the upper troposphere was set to a fixed relative humidity of 0.4. The stratospheric water vapor concentration was set to the profile's minimum. All other constituents were taken from the base RRTMG profile as described

---

Corresponding author: S. Bourguet, Department of Earth and Planetary Sciences, Harvard University, 20 Oxford Street, Cambridge, MA 02138, USA. (stephen_bourguet@g.harvard.edu)

in Kluft, Dacie, Buehler, Schmidt, and Stevens (2019). A zenith angle of 57.6 was used (Cronin, 2014), and the calculation was done with no diurnal cycle for 200 d with a timestep of 0.05 d. After reaching equilibrium, the temperature profile near the LZRH was smoothed to reduce jumps in the temperature profile.

References

Abalos, M., Randel, W., Kinnison, D., & Serrano, E. (2013). Quantifying tracer transport in the tropical lower stratosphere using waccm. *Atmospheric Chemistry and Physics*, *13*(21), 10591–10607. doi: 10.5194/acp-13-10591-2013

Cronin, T. W. (2014). On the choice of average solar zenith angle. *Journal of the Atmospheric Sciences*, *71*(8), 2994–3003.

Kluft, L., Dacie, S., Buehler, S. A., Schmidt, H., & Stevens, B. (2019). Re-examining the first climate models: Climate sensitivity of a modern radiative–convective equilibrium model. *Journal of Climate*, *32*(23), 8111–8125. doi: 10.1175/JCLI-D-18-0774.1

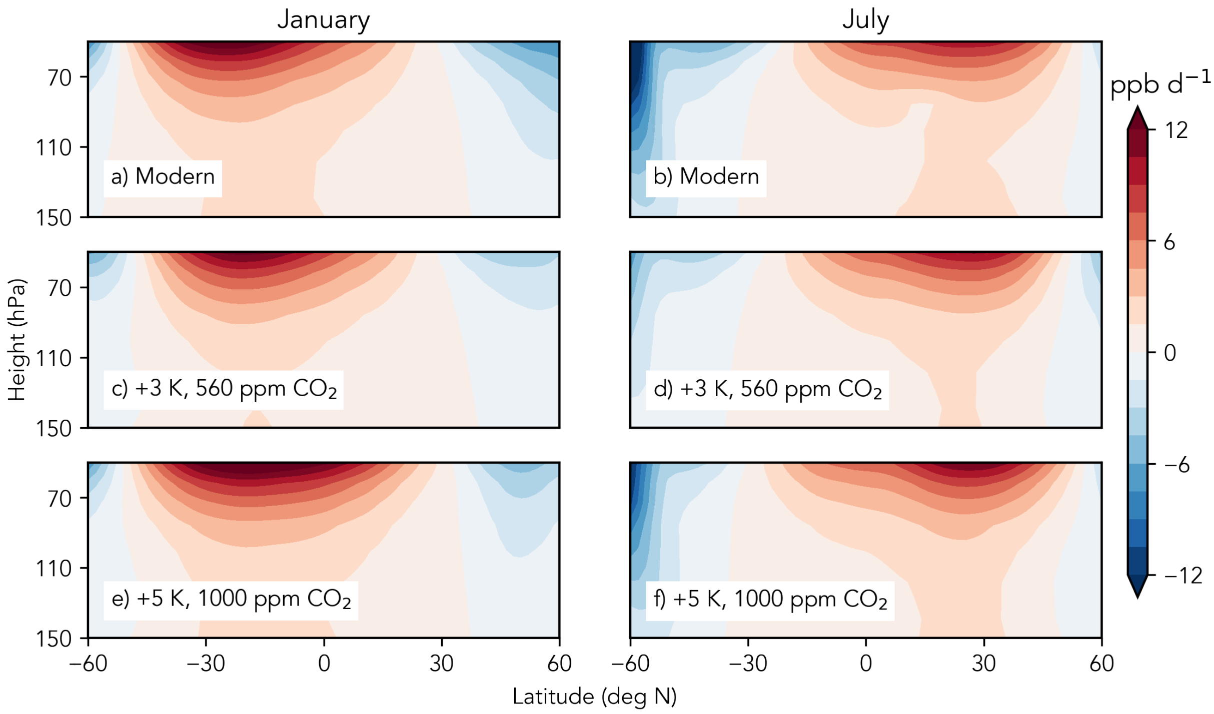

Figure S1. Zonal mean ozone production rates from WACCM January (left column) and July (right column). Modern rates were supplied by Marta Abalos (personal communication) and are described in Abalos et al. (2013). Simulations with increased CO_2 and surface temperatures were run with uniform surface warming.

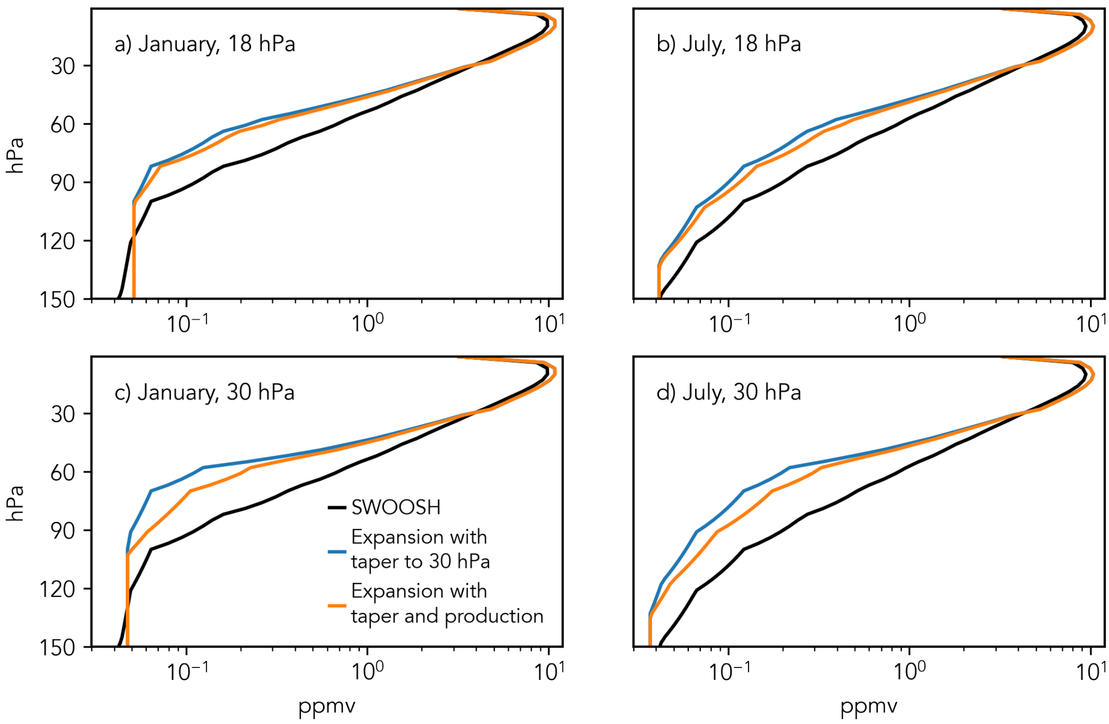

Figure S2. The 2002–2016 mean January and July ozone profile taken from SWOOSH (black line), and ozone profiles following 18 and 30 hPa of tropospheric expansion with and without increased ozone production (orange and blue, respectively). Panel c is the same as Figure 2 in the main text.

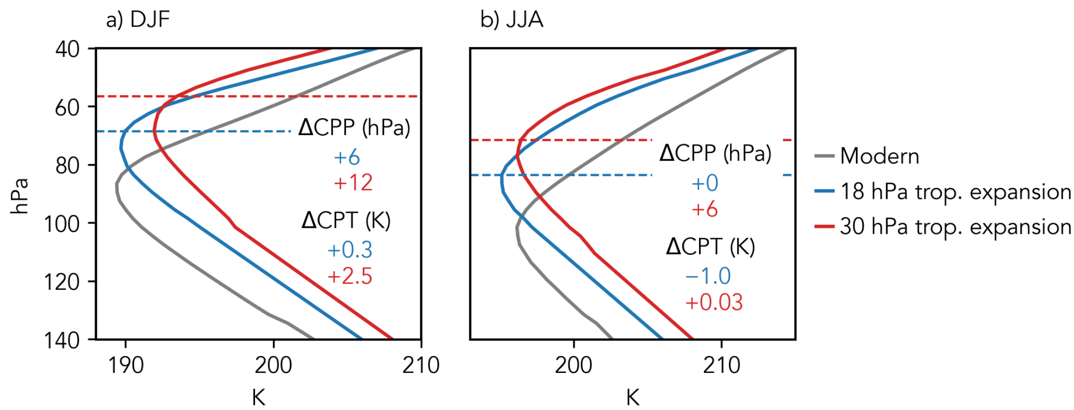

Figure S3. Temperature profiles for 18 hPa (blue) and 30 hPa (red) of tropospheric expansion in (a) DJF and (b) JJA, with the change in cold point temperature and pressure relative to a pure vertical shift listed. 30 hPa profiles are the same as in Figure 3 in the main text. The capping of the cold point tropopause becomes more pronounced as expansion progresses.

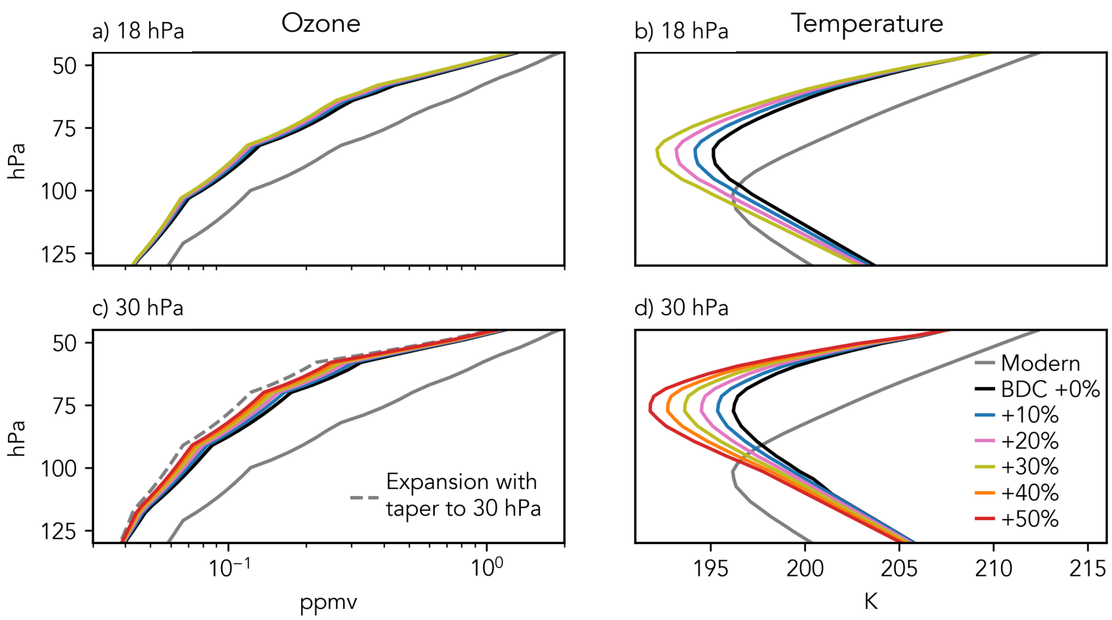

Figure S4. The effects of the BDC strength on lower stratospheric ozone (left column) and temperature (right column) profiles in JJA following 18 hPa (top row) and 30 hPa (bottom row) of tropospheric expansion. Details of the modified ozone profiles and radiative transfer calculations are described in the text, and corresponding profiles for DJF are shown in Figure 4.